Microstructure and mechanical properties of W_f/W composites influenced by Y_2O_3 coating

Rui Shu[a,b,*], Yiran Mao[a,d] , Jan W Coenen[a,e], Alexis Terra[a], Chao Liu[b], Stephan Schönen[f], Till Höschen[c], Johann Riesch[c], Christian Linsmeier[a] and Christoph Broeckmann[b]

[a] *Forschungszentrum Jülich GmbH, Institut für Energie- und Klimaforschung - Plasmaphysik, Partner in the Trilateral Euregio Cluster, 52425 Jülich, Germany*

[b] *Institut für Werkstoffanwendungen im Maschinenbau (IWM), RWTH Aachen University, 52062 Aachen, Germany*

[c] *Max-Planck-Institut für Plasmaphysik, 85748 Garching b. München, Germany*

[d] *School of Mechanical Engineering, Hefei University of Technology, Hefei 230009, China*

[e] *Department of Engineering Physics, University of Wisconsin Madison, WI 53706 Madison, USA*

[f] *Forschungszentrum Jülich GmbH, Zentralinstitut für Engineering, Elektronik und Analytik - Engineering und Technologie (ZEA-1) , 52425 Jülich, Germany*

*Corresponding author: r.shu@fz-juelich.de (Rui Shu).

Abstract: Tungsten fiber reinforced tungsten (W_f/W) composite is one of the candidates to improve the toughness of tungsten materials. Powder metallurgy is a potential method to produce W_f/W composites, but it may cause the recrystallization and grain growth of the reinforcing fibers during the high temperature sintering process. In the present work, a layer of Y_2O_3 is coated on the fiber surface by magnetron sputtering to protect the fibers and prevent recrystallization and abnormal growth of grains. W_f/W composites with and without Y_2O_3 coating were fabricated by a field assisted sintering technology (FAST) process. Microstructure and mechanical properties were characterized. The influence of the Y_2O_3 coating on the properties of the fiber was discussed in detail. The Y_2O_3 coating can effectively prevent recrystallization and abnormal grain growth of fibers during the sintering process. The W_f/W composites with Y_2O_3 coating shows higher strength and pseudo-ductile behavior.

Keywords: W_f/W composite; Y_2O_3 coating; Microstructure; Mechanical properties; Field assisted sintering technology.

1 Introduction

Tungsten (W) has a high melting point and excellent mechanical properties at high temperature. However, its application is limited by its poor ductility at room temperature and high ductile-brittle transition temperature [1,2]. In order to improve the toughness of W materials, fiber reinforced W composites were developed based on the extrinsic toughening mechanisms similar to the fiber reinforced ceramic composites [3–5].

The W fibers processed by severe plastic deformation have good ductility and very high tensile strength, due to the elongated fine grain structure from their drawing production process [6,7]. Hence, recrystallization of the fibers can cause the degradation of the advanced mechanical properties [8]. To improve the recrystallization resistance of the fibers, potassium doping is often used to pin the grain boundary. The potassium doped W fibers show a ductile behavior even after annealing at a high temperature of 2173 K [9,10]. A weak interface between fibers and matrix realizes the mechanisms of interface de-bonding, crack deflection and fiber bridging, leading to a pseudo-ductile behavior of the composite [11–13]. The ductile W fibers may contribute the most for the energy dissipation of W_f/W composites fracture [12]. Yttrium oxide (Y_2O_3) has been chosen as the interface material because of its good thermal and chemical stability [14] and low activation due to neuron irradiation [15,16].

Powder metallurgy is a commonly used method to prepare W_f/W composites. Short random fiber reinforced W_f/W composites [17–19] and continuous fiber reinforced W_f/W composites [12,20] have been produced by powder metallurgy methods. The sintering process is usually carried out at a temperature higher than the recrystallization temperature of W, and the W fiber may recover and recrystallize during the sintering process, resulting in a sharp decrease in its ductility and strength [9,21]. Therefore, it is necessary to prevent recrystallization and grain growth of the fiber during sintering process for ensuring the good toughness of W_f/W composites.

In this work, two different W_f/W composites with and without Y_2O_3 coating are prepared via field assisted sintering technology (FAST), respectively. The microstructure and mechanical properties of the W_f/W composites are characterized and analyzed. The influence of the Y_2O_3 coating on the sintering process and fiber properties has been discussed.

2 Experimental

2.1 Composites fabrication

W powders (OSRAM GmbH) and W weaves (Institute of Textile Technology (ITA), RWTH Aachen University) were used as the raw materials. The average particle size of W powders is 5 μm. As shown in Figure 1a, the W weaves were woven with warp fibers (150 μm) of a distance of ≈0.2 mm and weft fibers (50 μm) of a distance of ≈5 mm, more details about the weaves can be found in [22].

Firstly, the W weaves were coated with a Y_2O_3 layer (with the thickness of ≈1.6 μm) by magnetron sputtering. The magnetron sputtering process is similar as described in [15].

Alternatively raw W weaves without Y_2O_3 coating were used. Secondly, the samples were assembled into the graphite mold (with a diameter of 40 mm) by placing one layer of W powder and one layer of W weave alternately (totaling with 19 layers of W powders and 18 layers of W weaves) [20]. Each layer of W powder was 4.5 g and all the W weaves were arranged in one direction. In addition, graphite sheets were placed between the sample and the mold, aiming to reduce the damage of the mold surface and to ease the sample removal process. And two layers of tungsten sheet were used to separate the sample and graphite sheets in order to reduce the carbon contamination [17,23]. Finally, the samples were consolidated via the FAST process, with a heating rate of 100 ℃/min and a holding time of 5 min at 1800 ℃ (the temperature is measured at the bottom of the hollow punch) under 50 MPa. The composite was a commercial FAST system (HP D 25–2) from "FCT Systeme GmbH" (max force, 250 kN; max temperature, 2200 ℃; max heating rate, 400 K/min) is used in this study. The diagram of the sintering process and the final sample is shown as the Figure 1b.

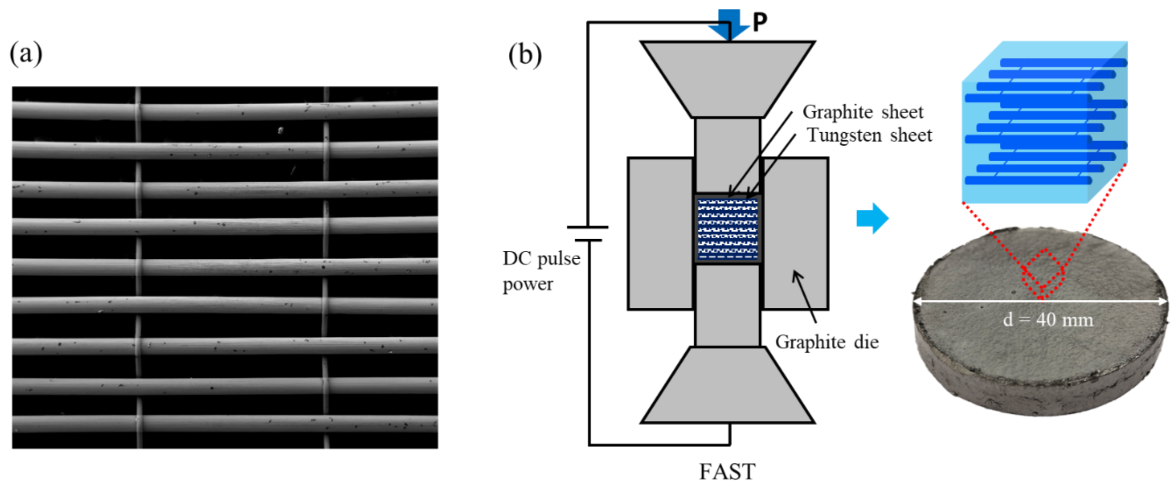

Figure 1. (a) W fiber weave; (b) Schematic diagram of the preparation process of the W_f/W composites.

2.2 Characterization

The mass density of the sintered W_f/W samples was measured by the Archimedes principle. The microstructure of the composites was analyzed via a LEO 982 scanning electron microscope (SEM) with an energy dispersive X-ray spectroscopy (EDX) system after mechanical polishing and OPS polishing. The grain sizes of the fibers in cross section (plane perpendicular to the drawing axis) and longitudinal section (plane parallel to the drawing axis) were statistically analyzed by measuring the diameter of grains.

Tensile tests and pre-notched 3-point bending test were used to measure the mechanical properties of the composites. Figure 2 illustrates the dimensions of the specimens. The dog-bone-shape tensile specimens have a gauge length of 13.5 mm and a cross section of 3 × 2 mm^2. The 3-point bending specimens are 27 mm × 3 mm × 4 mm (length × width × thickness) with a 1 mm deep V-notch (0.1 mm notch root radius) and the span between the holders is 25 mm. All specimens were manufactured by electrical discharged machining (EDM). The tensile tests and 3-point bending tests were performed using an Instron 3342 universal testing machine (Instron GmbH) with a displacement rate of 5 µm/s and 1 µm/s, respectively. During the tests, force and displacement were measured and the tests continued until complete failure of the specimen. The displacement is measured by an optical camera system [24]. Three tensile specimens and four 3-point bending specimens of each type of composites were prepared for each test. After mechanical testing, the microstructure of the fracture section is analyzed via SEM (LEO 982).

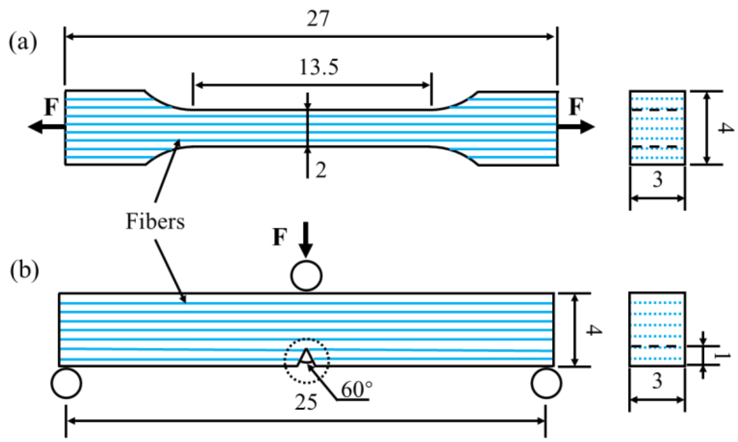

Figure 2. (a) Dimensions of specimen for tensile tests; (b) Dimensions of specimen for pre-notched 3-point bending tests.

3 Results and discussion

3.1 Microstructure of the W_f/W composites

The relative densities of the W_f/W composites are 92.87% (with Y_2O_3 coating) and 92.57% (without Y_2O_3 coating), respectively. The Y_2O_3 coating shows little effect on the sintering density of the samples. Figures 3 and 5 show the microstructure of the prepared W_f/W composites. No matter for the composites with or without Y_2O_3 coating, the fibers can be clearly distinguished from the matrix, although there is no interlayer phase between the fibers and matrix anymore. The matrix of both composites has the similar microstructure, and there are many pores on the boundary of grains which is similar to the report in [21], it is consistent with the values of relative density. It indicates that Y_2O_3 coating has little effect on the microstructure of the matrix. However, the microstructure of the fibers is much different. The original grains in cross-section of the as-fabricated fibers have a curled structure and sizes in range of (0.1-0.4) × (0.5-1) μm^2 [8]. While as shown in Figures 3b and 3c, the fiber in the W_f/W composite with Y_2O_3 coating has fine and uniform equiaxed grains, with the sizes in range of 0.8-4 μm. These grains are columnar and they have a larger size on the axial direction of the fiber (as shown in Figure 3d), they maintain a high aspect ratio and the grain size along the fiber direction is approximately 2-30 μm (the original grain size was estimated to be 10-40 μm [8]). It indicates that recrystallization and grain growth occurred during the sintering process, equivalent to the heat treatment of W fibers and the fiber grain size in this sample is similar to the pure W wire after 1200℃/1h heat treatment in [25]. The fiber contact tightly with the matrix and no Y_2O_3 layer observed on the interface (Figure 3b). The disappearance of the Y_2O_3 layer between fibers and matrix can be attributed to the high temperature and pressure conditions during the FAST process, and the dielectric breakdown [3,26]. The pulsed current could produce electrical discharge and remove the surface oxide layer, and increasing heating rate will in general lead to the increase of the electrical discharge [27,28]. As shown in Figures 3e and 3f, some Y_2O_3 particles were observed in the matrix in the vicinity of the fibers, these particles are embedded between matrix grains and irregular in shape and size.

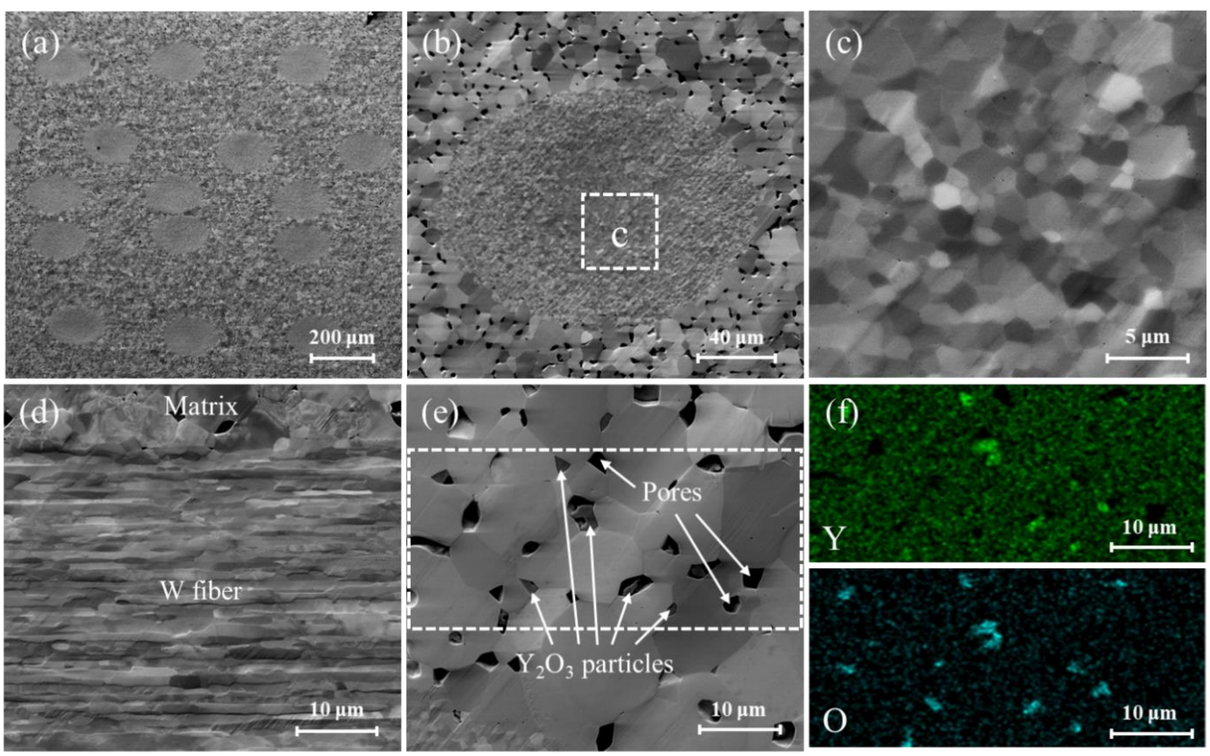

Figure 3. Microstructure of the W_f/W composites with Y_2O_3 coating: (a-c) cross-section

perpendicular to the direction of fiber alignment; (d) longitudinal section of the W fiber; (e) microstructure of the matrix in the vicinity of the fiber; (f) distributions of the elements Y and O in the dotted region in (e) by EDX mapping analysis.

The Y_2O_3 coating produced by the magnetron sputtering is a stable cubic phase [15]. Therefore the disappearance of Y_2O_3 coating could be consider as a physical process (The continuous Y_2O_3 coating damaged into small particles, which move and disperse into the adjacent matrix.), it could be illustrated as Figure 4. At the beginning, the Y_2O_3 coating has an intact microstructure and no electric current pass through it due to its excellent electrical insulation (Figure 4a). While the plasma and local Joule heating may form at the surface based on the pulsed current, which can increase the material densification process as well as the damage of Y_2O_3 coating [29–31]. With the increase of pressure and temperature, some cracks may generate and the broken Y_2O_3 particles could move along with the movement of W powders (Figure 4b). If the coating is completely damaged before the end of sintering process, the current will pass though the fiber (Figure 4c).

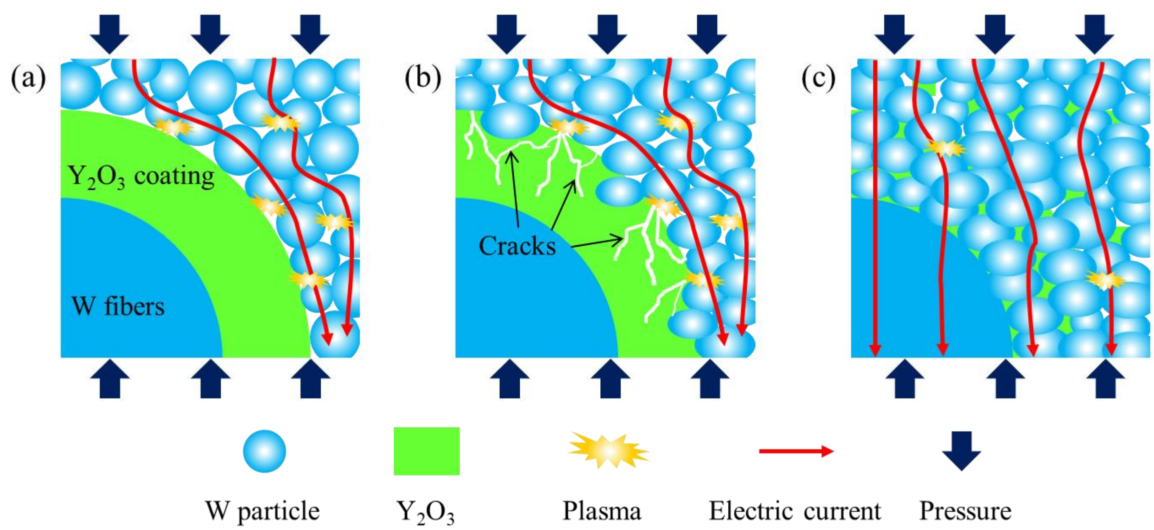

Figure 4. Schematic diagram of the microstructural evolution of Y_2O_3 coating during the sintering process.

Figure 5 reveals the microstructure of the W_f/W composite without Y_2O_3 coating. The grains in the periphery zone of the fiber are equiaxed grains and have the sizes in a range of 5-30 μm, the grain size increases obviously because of the recrystallization and abnormal growth during sintering process. The grain size of the central zone also has a little increase (1-8 μm) but they still have a high aspect ratio (although the aspect ratio is lower than that in the W_f/W composites with Y_2O_3 coating, as shown in Figures 5d and 5e). The difference of the grain size between the central zone and the periphery zone could be attributed to the higher local temperature of the periphery zone caused by the high contact resistance at the fiber-matrix interface. It strongly indicates that Y_2O_3 coating can effectively prevent the abnormal grain growth of W fibers during the SPS process. One interesting phenomenon is that the microstructure of the W_f/W composites without Y_2O_3 coating is much different from the report in [12]. The latter produced the single layer fiber reinforced W_f/W composites without Y_2O_3 interface under a lower heating rate (50 °C/min). Some researchers also find that the grain size decreased with increasing heating rate [32,33]. The higher heating rate usually corresponds to the higher electric current intensity, and the higher current density is conducive to mass transport and grain growth [27,34]. More details of the effects of sintering parameters on the Y_2O_3 interface and the microstructure of the fiber will be further investigated in future work.

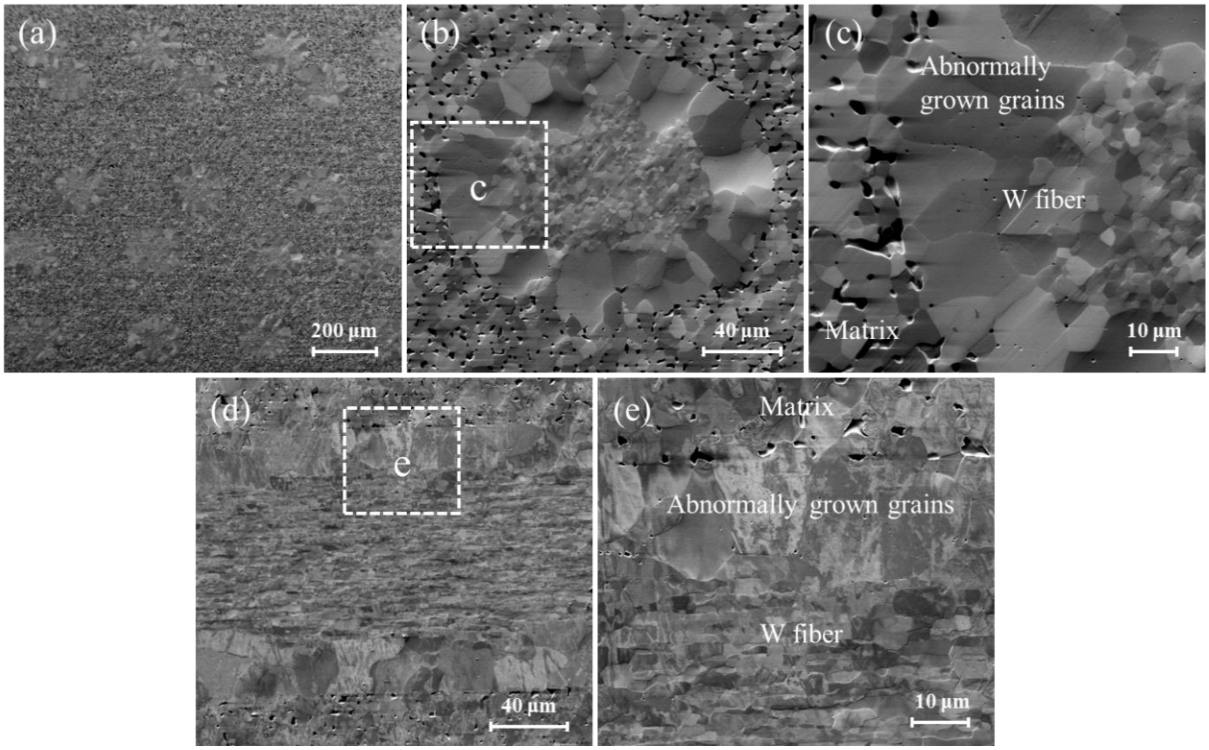

Figure 5. Microstructure of the W_f/W composites without Y_2O_3 coating: (a-c) cross-section perpendicular to the direction of fiber alignment; (d-e) longitudinal section of the W fiber.

Figure 6 illustrates the diagram of the simplified current conditions at the beginning of sintering. It just displays the main current state (in the real case there is a part of the current along the fiber). For the composite with Y_2O_3 coating (Figure 6a), due to the existence of the electrically insulating Y_2O_3 coating, the current could not pass through the fibers and no Joule heat generated in them. Therefore, the fine grain size of fibers is maintained after sintering. However, the current can pass through the fibers directly if there is no interface (Figure 6b), and with a higher contact resistance on the fiber surface, more Joule heat will be generated, resulting in a high local temperature and thus significant grain growth. At the same time, the current can also enhance the atom diffusivity and therefore accelerate the grain growth [35]. As the sintering progresses, the Y_2O_3 coating layer will be destroyed and the current will also pass through the fibers in the W_f/W composites with Y_2O_3 coating (as shown in Figure 4c), but it has little effect on the recrystallization and grain growth because the duration is significantly shorter compared to the case without Y_2O_3 interface. This is a possible explanation to lead to the different fiber microstructures in Figures 3 and 5. More details and mechanisms of the sintering process will be investigated in future works.

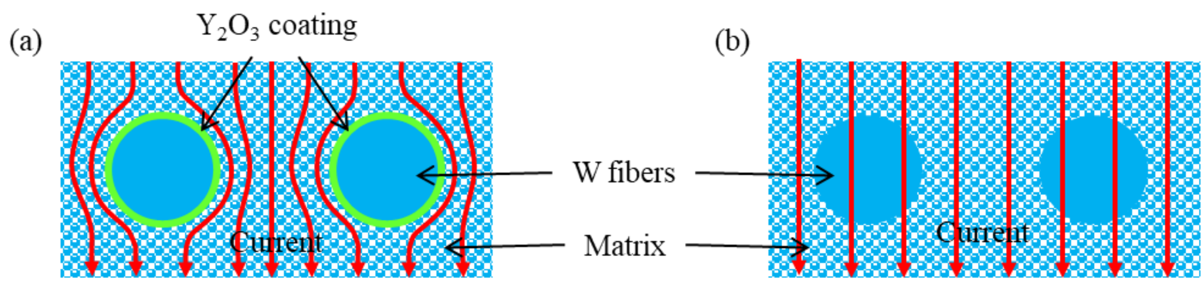

Figure 6. Diagram of the current conditions during the sintering process (red arrows indicate the current): (a) with Y_2O_3 coating; (b) without Y_2O_3 coating.

3.2 Mechanical properties by tensile tests

Table 1 reveals some results of the tensile test. It is clear that both the W_f/W composites have a similar Young's modulus (≈306 GPa and ≈307 GPa, respectively), which is lower than the theoretical value of pure W (400 GPa) due to the lower relative density. The porous microstructure of matrix could lead to a decreased Young's modulus [36]. The W_f/W composite with Y_2O_3 coating shows higher tensile strength (≈289 MPa) and fracture strain (≈0.095%) than the W_f/W composite without Y_2O_3 coating (≈243 MPa and ≈0.082%, respectively). As shown in Figure 7, the tensile stress-strain curves are noisy and end at the maximum stress. The noise of the curves are caused by the camera system which used to track the test process. The curves of both W_f/W composites with or without Y_2O_3 coating show a linear trend, means that all test samples of both composites only have elastic deformation during the test process, so the maximum strain is correlated with the strength. Moreover, the fracture surface is flat and perpendicular to the load direction.

Table 1. Mechanical properties of the W_f/W composites by tensile test.

Samples	Young's Modulus (GPa)	Tensile strength (MPa)	Fracture strain (%)
W_f/W with Y_2O_3 coating	306.29±10.51	289.52±23.83	0.0947±0.0093
W_f/W without Y_2O_3 coating	307.53±13.62	243.44±32.10	0.0820±0.0065
CVD W_f/W in [37]	-	482	≈3.47
		557	≈3.83

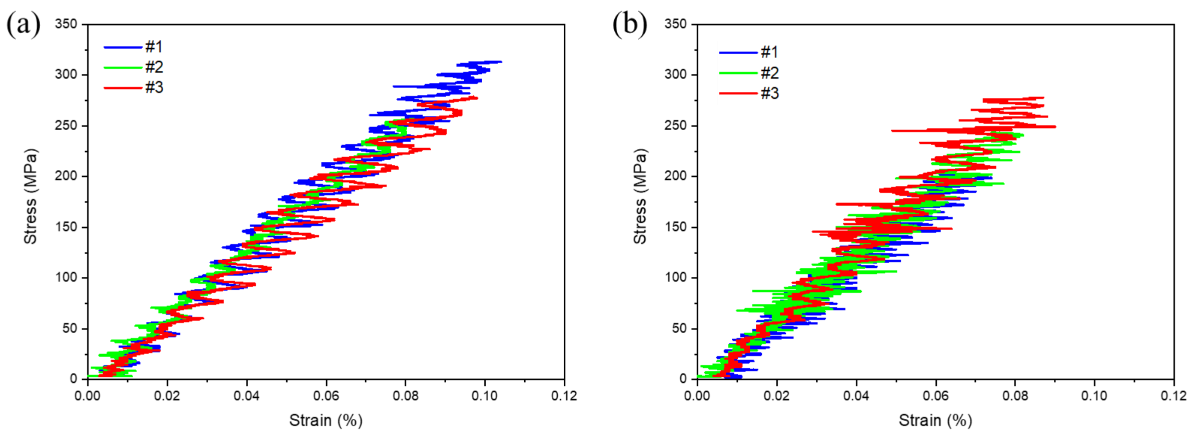

Figure 7. Stress-strain curves of the W_f/W composites by tensile test: (a) with Y_2O_3 coating; (b) without Y_2O_3 coating.

Figure 8 shows the SEM morphology of the tensile fracture surfaces of the W_f/W composites. There are many pores in the matrix, which correspond to the relative density of the composites mentioned above. The crack mainly propagates along the boundary between W particles, i.e. intergranular fracture. The only difference between the matrixes is that there are some Y_2O_3 particles existing in the matrix of the W_f/W composite with Y_2O_3 coating (Figure 8c). In contrast to the matrix, the fibers in both composites show different fracture mechanisms. The fiber in the

W_f/W composite with Y_2O_3 coating has a microstructure of fine columnar grains and fractures with the mechanism of transgranular fracture with cleavage pattern (as shown in Figures 8b and 8c). Figure 8c reveals the detail of the fiber-matrix boundary, the fiber is tightly in contact with the matrix. There is no observation of the existence of Y_2O_3 layer and cracks on the interface, it is a complete W-W boundary. From Figures 8e and 8f, a difference of the fracture mechanisms can be observed between the central zone (intergranular fracture and transgranular fracture) and periphery zone (intergranular fracture) of the fiber in the W_f/W composite without Y_2O_3 coating. Both PM W_f/W composites prepared in the present work show lower strength and toughness than the CVD W_f/W composites reported in [37]. On the one hand, they have lower compactness and the pores in the matrix reduce the effective cross-sectional area and may act as crack sources, thus the matrix has a low strength. On the other hand, the strong W-W boundary could limit the plastic deformation of the fibers (even though the fiber has plasticity) [12,38].

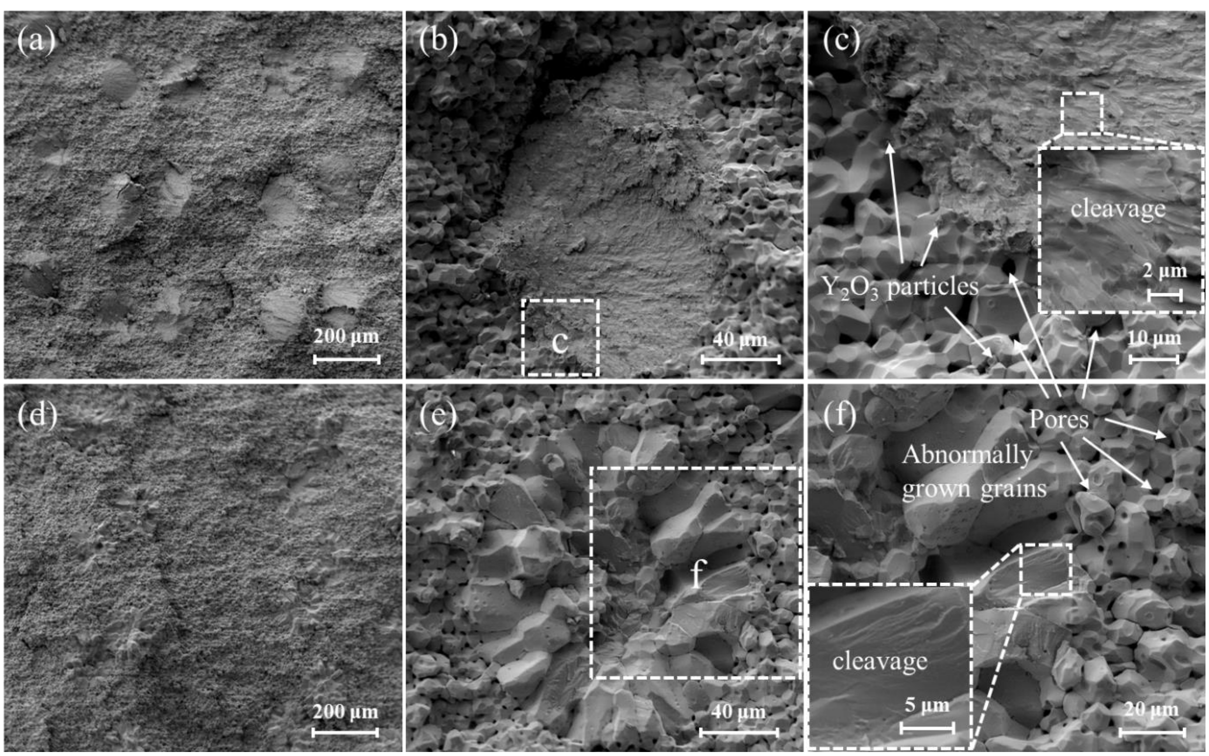

Figure 8. SEM images of the tensile fracture surfaces of the W_f/W composites: (a-c) with Y_2O_3 coating; (d-f) without Y_2O_3 coating.

As the interfaces between fibers and matrix have a high strength and do not de-bonding occurred during the tensile tests, the tensile strength (σ_c) can be estimated with the strength of the matrix (σ_m) and the fiber (σ_f) and the volume fraction of the matrix (v_m) and the fiber (v_f) by following equation [39]:

$$\sigma_c = \sigma_m v_m + \sigma_f v_f \quad (1)$$

The tensile strength of the matrix can be regarded as the strength of pure W produced via the same method, which is σ_m = 239 MPa [40]. Both W_f/W composites have the same volume fraction of the fiber, $v_f \approx 20\%$, thus $v_m \approx 80\%$. Therefore, the strength of the fiber in the W_f/W composite with Y_2O_3 coating ($\sigma_{f-with\,coating}$) and the W_f/W composite without Y_2O_3 coating ($\sigma_{f-without\,coating}$) can be calculated by:

$$\sigma_f = \frac{\sigma_c - \sigma_m v_m}{v_f} \quad (2)$$

Substituting the tensile strength values in Table 1 into the Eq. (2), we can achieve that $\sigma_{f-with\,coating}$ = 491.6 MPa and $\sigma_{f-without\,coating}$ = 261.2 MPa. The strength of the W fiber without the protection of Y_2O_3 coating shows a great decrease (almost half of the one with protection), although the spread in the tensile values may cause an error to the values of fiber strength. It shows that the Y_2O_3 coating has a great effect on the microstructure and mechanical properties of the W fiber during FAST process. The transformation of the microstructure of fibers will greatly reduce its mechanical properties [8,41]. The values of the strength are much lower than the strength of the W fiber reported in previous researches [6,8], which indicates that the properties of W fibers may have some decrease during the preparation of W_f/W composites.

3.3 Fracture behavior by 3-point bending tests

The fracture behavior of the composites was tested by a pre-notched 3-point bending test. Figure 9 shows the force-displacement curves of the test results. Comparing between Figure 9a and 9b, the maximum force of the W_f/W composite with Y_2O_3 coating (≈ 220 N) is higher than the one of the W_f/W composite without Y_2O_3 coating (≈ 130 N), although it does not represent the strength of the samples because of the existence of the pre-fabricated notch. For the W_f/W composite with Y_2O_3 coating (Figure 9a), the force increases approximately linearly with the displacement, it is an elastic process. Next, the load drops suddenly after reaching the maximum force, it is accompanied by the unstable propagation of the crack. And then, keeping a load about 70 N for a long displacement. As shown in Figure 9b, the curves of the W_f/W composite without Y_2O_3 coating show an elastic stage followed by a slight displacement with a decreased slope before the maximum force. However, the load gradually decreases after the maximum force is reached. The maximum force and displacement is much lower than the previous one. It means the difference of strength between the fiber and the matrix is smaller and it has lower fracture energy dissipation. In the tests of both W_f/W composites, a stable crack propagation process has been observed before the maximum force, thus the curves show a slop decrease and this crack length would be used to calculate the fracture toughness of the samples.

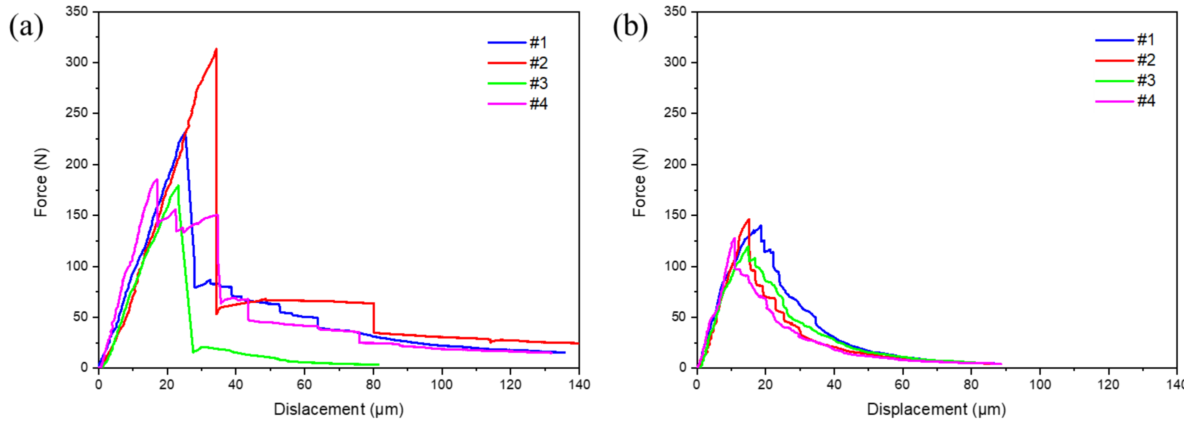

Figure 9. Force-Displacement curves of the W_f/W composites by pre-notched 3-point bending test: (a) with Y_2O_3 coating; (b) without Y_2O_3 coating.

Figure 10 shows the morphology of the fracture surface of the W_f/W composite with Y_2O_3 coating tested by the pre-notched 3-point bending test. The samples show a macroscopically flat fracture surface, which means that the crack did not deflect significantly during the test. The fibers fracture with a brittle manner, where river patterns can be observed on the fracture (Figure 10c). During the fracture process, the fibers will suffer with a triaxial tensile stress, because the bonding strength between fibers and matrix is too high to enable de-bonding. The fiber tend to fail brittle under this loading state even it has good plasticity [38,42]. The fibers are in tight contact with the matrix, but there are also some cracks on the interface. It may be caused by the huge difference between the strength of fibers and matrix. The crack can generate easier in the weaker matrix and propagate across the stronger fibers.

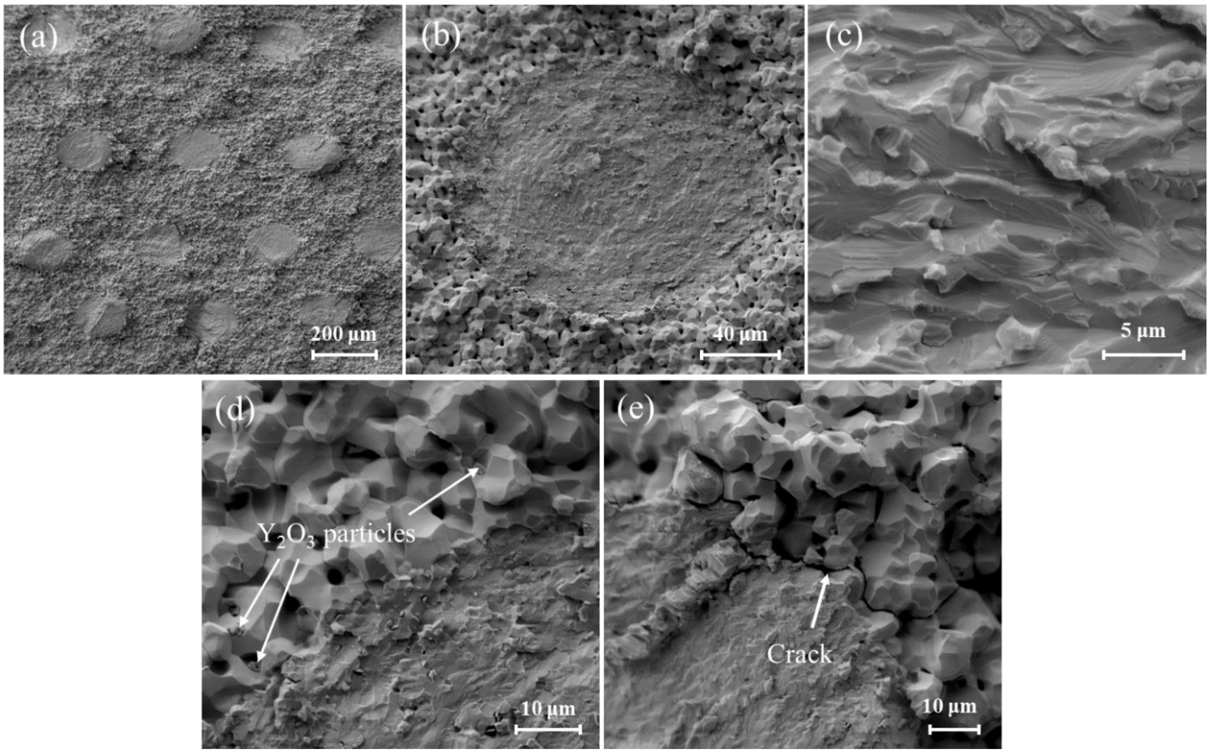

Figure 10. Bending fracture surface of the W_f/W composite with Y_2O_3 coating.

For the W_f/W composite without Y_2O_3 coating (Figure 11), the fracture surface is also macroscopically flat and similar with the tensile fracture surface (Figures 8d-f). It is a complete brittle fracture. The periphery zone of the fiber is fully intergranular fracture as well as the matrix (Figure 11b). The central zone of the fiber is a combination of intergranular fracture and transgranular fracture (Figure 11c).

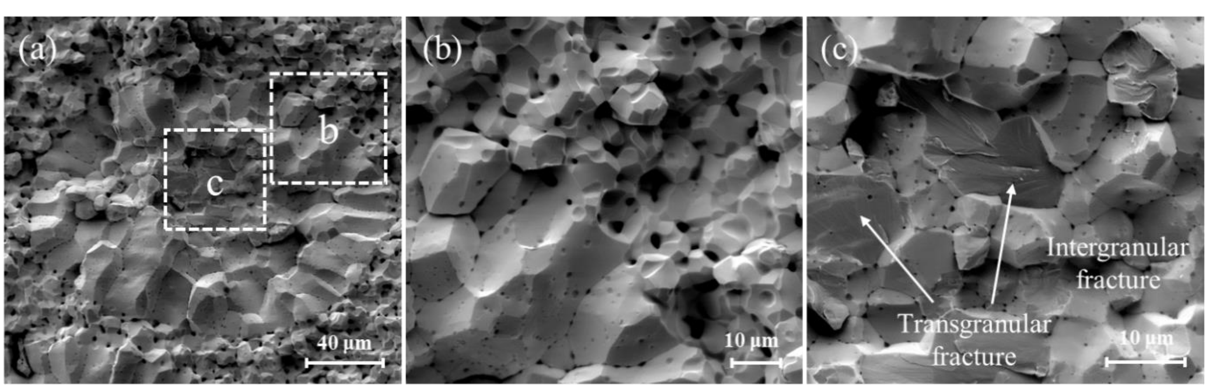

Figure 11. Bending fracture surface of the W_f/W composite without Y_2O_3 coating.

Based on the pre-notched 3-point bending tests, fracture energy density and fracture toughness were calculated and shown in Table 2. The values are all higher than that of pure W in [24], which means the toughness of the W material could be improved by the addition of W fibers. The W_f/W composite with Y_2O_3 coating has higher fracture energy density and fracture toughness, which is 0.88 ± 0.10 kJ·m^{-2} and 14.32 ± 2.63 MPa·m$^{0.5}$, respectively. It is mainly attributed to higher strength of the fiber. Compared with the CVD W_f/W composites in [43], the fracture toughness of the W_f/W composite with Y_2O_3 coating is lower than the value of CVD as-fabricated W_f/W_{Y2O3} (206 ± 29 MPa·m$^{0.5}$) and similar to the CVD embrittled W_f/W_{Y2O3} (14 ± 1 MPa·m$^{0.5}$). It is consistent with the results that the fibers fracture in a brittle manner, but the brittle fracture of fibers in present work is caused by the stress state during the test process [42]. It indicates that a weak interface is necessary to realize the toughening effect of the ductile fiber.

Table 2. Fracture energy density and fracture toughness of the W_f/W composites.

Samples	Fracture energy density (kJ·m^{-2})	Fracture toughness, Kq (MPa·m$^{0.5}$)
W_f/W with Y_2O_3 coating	0.88±0.10	14.32±2.63
W_f/W without Y_2O_3 coating	0.32±0.04	8.73±0.54
Pure W in [24]	≈0.12	≈5.55

The existence of the Y_2O_3 coating can effectively prevent the recrystallization and abnormal grain growth of the fiber, thereby reducing the reduction of the strength of the fiber caused by the sintering process. However, due to the disappearance of the Y_2O_3 coating after sintering, a strong W-W boundary between the fiber and the matrix is formed. Therefore, no interface de-bonding and thus there is no plastic deformation of fibers during the fracture process. The improvement of the toughness is mainly contributed by the high strength of the fiber, as well as the resistance of the fiber to crack propagation.

4 Conclusion

The bulk continuous fiber reinforced W_f/W composites were fabricated by field assisted sintering technology with the W fibers with and without Y_2O_3 coating protection, respectively. The Y_2O_3 coating damaged and dispersed into the surrounding matrix during the sintering process due to the assisted pulsed current. Nevertheless the insulating Y_2O_3 coating can effectively prevent the high local temperature on the fiber surface caused by the current in the sintering process. By this, the Y_2O_3 coating can protect fibers from recrystallization and abnormal grain growth. The composite with Y_2O_3 coating has higher strength (≈289 MPa) and strain (≈0.095%), and also higher fracture energy density (≈0.88 $kJ \cdot m^{-2}$) and fracture toughness (≈14.32 $MPa \cdot m^{0.5}$). The W fibers without Y_2O_3 coating show recrystallization and abnormal grain growth in the periphery zone at the present sintering parameters. It could be attributed to the high current intensity and the high local temperature caused by the high contact resistance at the interface. Further investigation on the influence of the coating and sintering parameters on the microstructure and properties of W_f/W composites will be carried out in future.

Acknowledgements

This work has been carried out within the framework of the EUROfusion Consortium, funded by the European Union via the Euratom Research and Training Programme (Grant Agreement No 101052200 - EUROfusion). Rui Shu is financially supported by China Scholarship Council (CSC) with No. 202007000034. Views and opinions expressed are however those of the author(s) only and do not necessarily reflect those of the European Union or the European Commission. Neither the European Union nor the European Commission can be held responsible for them.

References

[1] C. Ren, Z.Z. Fang, M. Koopman, B. Butler, J. Paramore, S. Middlemas, Methods for improving ductility of tungsten - A review, Int. J. Refract. Met. Hard Mater. 75 (2018) 170–183. https://doi.org/10.1016/j.ijrmhm.2018.04.012.

[2] Y.H. Zhang, W.Z. Han, Mechanism of brittle-to-ductile transition in tungsten under small-punch testing, Acta Mater. 220 (2021) 117332. https://doi.org/10.1016/J.ACTAMAT.2021.117332.

[3] Y. Mao, J.W. Coenen, J. Riesch, S. Sistla, J. Almanstötter, B. Jasper, A. Terra, T. Höschen, H. Gietl, M. Bram, J. Gonzalez-Julian, C. Linsmeier, C. Broeckmann, Development and characterization of powder metallurgically produced discontinuous tungsten fiber reinforced tungsten composites, Phys. Scr. 2017 (2017). https://doi.org/10.1088/0031-8949/2017/T170/014005.

[4] L.H. Zhang, Y. Jiang, Q.F. Fang, T. Zhang, X.P. Wang, C.S. Liu, Toughness and microstructure of tungsten fibre net-reinforced tungsten composite produced by spark plasma sintering, Mater. Sci. Eng. A. 659 (2016) 29–36. https://doi.org/10.1016/j.msea.2016.02.034.

[5] Y. Mao, J. Coenen, S. Sistla, C. Liu, A. Terra, X. Tan, J. Riesch, T. Hoeschen, Y. Wu, C. Broeckmann, C. Linsmeier, Design of tungsten fiber-reinforced tungsten composites with porous matrix, Mater. Sci. Eng. A. 817 (2021) 141361.

https://doi.org/10.1016/j.msea.2021.141361.

[6] J. Riesch, A. Feichtmayer, M. Fuhr, J. Almanstötter, J.W. Coenen, H. Gietl, T. Höschen, C. Linsmeier, R. Neu, Tensile behaviour of drawn tungsten wire used in tungsten fibre-reinforced tungsten composites, Phys. Scr. 2017 (2017). https://doi.org/10.1088/1402-4896/aa891d.

[7] J. Riesch, J. Almanstötter, J.W. Coenen, M. Fuhr, H. Gietl, Y. Han, T. Höschen, C. Linsmeier, N. Travitzky, P. Zhao, R. Neu, Properties of drawn W wire used as high performance fibre in tungsten fibre-reinforced tungsten composite, IOP Conf. Ser. Mater. Sci. Eng. 139 (2016). https://doi.org/10.1088/1757-899X/139/1/012043.

[8] P. Zhao, J. Riesch, T. Höschen, J. Almanstötter, M. Balden, J.W. Coenen, R. Himml, W. Pantleon, U. von Toussaint, R. Neu, Microstructure, mechanical behaviour and fracture of pure tungsten wire after different heat treatments, Int. J. Refract. Met. Hard Mater. 68 (2017) 29–40. https://doi.org/10.1016/j.ijrmhm.2017.06.001.

[9] J. Riesch, Y. Han, J. Almanstötter, J.W. Coenen, T. Höschen, B. Jasper, P. Zhao, C. Linsmeier, R. Neu, Development of tungsten fibre-reinforced tungsten composites towards their use in DEMO - Potassium doped tungsten wire, Phys. Scr. 2016 (2016) 14006. https://doi.org/10.1088/0031-8949/T167/1/014006.

[10] D. Terentyev, J. Riesch, S. Lebediev, T. Khvan, A. Dubinko, A. Bakaeva, Strength and deformation mechanism of tungsten wires exposed to high temperature annealing: Impact of potassium doping, Int. J. Refract. Met. Hard Mater. 76 (2018) 226–233. https://doi.org/10.1016/j.ijrmhm.2018.07.002.

[11] K. Cui, Y. Zhang, T. Fu, J. Wang, X. Zhang, Toughening mechanism of mullite matrix

composites: A review, Coatings. 10 (2020). https://doi.org/10.3390/coatings10070672.

[12] R. Shu, Y. Mao, J.W. Coenen, A. Terra, C. Liu, S. Schönen, J. Riesch, C. Linsmeier, C. Broeckmann, Interface and Mechanical Properties of the Single-Layer Long Fiber Reinforced Wf/W Composites Fabricated Via Field Assisted Sintering Technology, Mater. Sci. Eng. A. 857 (2022). https://doi.org/10.1016/j.msea.2022.144098.

[13] J.P. Singh, D. Singh, M. Sutaria, Ceramic composites: roles of fiber and interface, Compos. Part A Appl. Sci. Manuf. 30 (1999) 445–450. https://doi.org/10.1016/S1359-835X(98)00133-X.

[14] P.P. Bose, M.K. Gupta, R. Mittal, S. Rols, S.N. Achary, A.K. Tyagi, S.L. Chaplot, Phase transitions and thermodynamic properties of yttria, Y 2O3: Inelastic neutron scattering shell model and first-principles calculations, Phys. Rev. B - Condens. Matter Mater. Phys. 84 (2011) 1–11. https://doi.org/10.1103/PhysRevB.84.094301.

[15] Y. Mao, J. Engels, A. Houben, M. Rasinski, J. Steffens, A. Terra, C. Linsmeier, J.W. Coenen, The influence of annealing on yttrium oxide thin film deposited by reactive magnetron sputtering: Process and microstructure, Nucl. Mater. Energy. 10 (2017) 1–8. https://doi.org/10.1016/j.nme.2016.12.031.

[16] S. Palaniyappan, M. Trautmann, Y. Mao, J. Riesch, P. Gowda, N. Rudolph, J.W. Coenen, R. Neu, G. Wagner, Yttria-coated tungsten fibers for use in tungsten fiber-reinforced composites: A comparative study on pvd vs. cvd routes, Coatings. 11 (2021). https://doi.org/10.3390/coatings11091128.

[17] J.W. Coenen, Y. Mao, S. Sistla, J. Riesch, T. Hoeschen, C. Broeckmann, R. Neu, C. Linsmeier, Improved pseudo-ductile behavior of powder metallurgical tungsten short

fiber-reinforced tungsten (Wf/W), Nucl. Mater. Energy. 15 (2018) 214–219. https://doi.org/10.1016/j.nme.2018.05.001.

[18] Y. Jiang, L.H. Zhang, Q.F. Fang, T. Zhang, X.P. Wang, T. Hao, C.S. Liu, Toughness enhancement of tungsten reinforced with short tungsten fibres, Mater. Sci. Eng. A. 690 (2017) 208–213. https://doi.org/10.1016/j.msea.2017.02.106.

[19] Y. Mao, J.W. Coenen, S. Sistla, X. Tan, J. Riesch, L. Raumann, D. Schwalenberg, T. Höschen, C. Chen, Y. Wu, C. Broeckmann, C. Linsmeier, Development of tungsten fiber-reinforced tungsten with a porous matrix, Phys. Scr. 2020 (2020). https://doi.org/10.1088/1402-4896/ab482e.

[20] Y. Mao, J.W. Coenen, C. Liu, A. Terra, X. Tan, J. Riesch, T. Höschen, Y. Wu, C. Broeckmann, C. Linsmeier, Powder Metallurgy Produced Aligned Long Tungsten Fiber Reinforced Tungsten Composites, J. Nucl. Eng. 3 (2022) 446–452.

[21] S. Deng, T. Yuan, R. Li, F. Zeng, G. Liu, X. Zhou, Spark plasma sintering of pure tungsten powder: Densification kinetics and grain growth, Powder Technol. 310 (2017) 264–271. https://doi.org/10.1016/j.powtec.2017.01.050.

[22] H. Gietl, A. V. Müller, J.W. Coenen, M. Decius, D. Ewert, T. Höschen, P. Huber, M. Milwich, J. Riesch, R. Neu, Textile preforms for tungsten fibre-reinforced composites, J. Compos. Mater. 52 (2018) 3875–3884. https://doi.org/10.1177/0021998318771149.

[23] Y. Mao, C. Chen, J.W. Coenen, J. Riesch, S. Sistla, J. Almanstötter, A. Terra, Y. Wu, L. Raumann, T. Höschen, H. Gietl, R. Neu, C. Linsmeier, C. Broeckmann, On the nature of carbon embrittlement of tungsten fibers during powder metallurgical processes, Fusion Eng. Des. 145 (2019) 18–22. https://doi.org/10.1016/j.fusengdes.2019.05.033.

[24] Y. Mao, J.W. Coenen, J. Riesch, S. Sistla, J. Almanstötter, J. Reiser, A. Terra, C. Chen, Y. Wu, L. Raumann, T. Höschen, H. Gietl, R. Neu, C. Linsmeier, C. Broeckmann, Fracture behavior of random distributed short tungsten fiber-reinforced tungsten composites, Nucl. Fusion. 59 (2019) 1–28. https://doi.org/10.1088/1741-4326/ab25b0.

[25] V. Nikolić, J. Riesch, R. Pippan, The effect of heat treatments on pure and potassium doped drawn tungsten wires: Part I - Microstructural characterization, Mater. Sci. Eng. A. 737 (2018) 422–433. https://doi.org/10.1016/j.msea.2018.09.027.

[26] C.S. Bonifacio, T.B. Holland, K. Van Benthem, Time-dependent dielectric breakdown of surface oxides during electric-field-assisted sintering, Acta Mater. 63 (2014) 140–149. https://doi.org/10.1016/j.actamat.2013.10.018.

[27] Z.A. Munir, U. Anselmi-Tamburini, M. Ohyanagi, The effect of electric field and pressure on the synthesis and consolidation of materials: A review of the spark plasma sintering method, J. Mater. Sci. 41 (2006) 763–777. https://doi.org/10.1007/s10853-006-6555-2.

[28] X.P. Li, M. Yan, H. Imai, K. Kondoh, G.B. Schaffer, M. Qian, The critical role of heating rate in enabling the removal of surface oxide films during spark plasma sintering of Al-based bulk metallic glass powder, J. Non. Cryst. Solids. 375 (2013) 95–98. https://doi.org/10.1016/j.jnoncrysol.2013.05.001.

[29] D.M. Hulbert, A. Anders, J. Andersson, E.J. Lavernia, A.K. Mukherjee, A discussion on the absence of plasma in spark plasma sintering, Scr. Mater. 60 (2009) 835–838. https://doi.org/10.1016/j.scriptamat.2008.12.059.

[30] R. Marder, C. Estournès, G. Chevallier, R. Chaim, Plasma in spark plasma sintering of ceramic particle compacts, Scr. Mater. 82 (2014) 57–60.

https://doi.org/10.1016/j.scriptamat.2014.03.023.

[31] T.B. Holland, U. Anselmi-Tamburini, D. V. Quach, T.B. Tran, A.K. Mukherjee, Effects of local Joule heating during the field assisted sintering of ionic ceramics, J. Eur. Ceram. Soc. 32 (2012) 3667–3674. https://doi.org/10.1016/j.jeurceramsoc.2012.02.033.

[32] E. Autissier, M. Richou, L. Minier, F. Naimi, G. Pintsuk, F. Bernard, Spark plasma sintering of pure and doped tungsten as plasma facing material, Phys. Scr. T159 (2014). https://doi.org/10.1088/0031-8949/2014/T159/014034.

[33] G. Lee, E.A. Olevsky, C. Manière, A. Maximenko, O. Izhvanov, C. Back, J. McKittrick, Effect of electric current on densification behavior of conductive ceramic powders consolidated by spark plasma sintering, Acta Mater. 144 (2018) 524–533. https://doi.org/10.1016/j.actamat.2017.11.010.

[34] N. Bertolino, J. Garay, U. Anselmi-Tamburini, Z.A. Munir, Electromigration effects in Al-Au multilayers, Scr. Mater. 44 (2001) 737–742. https://doi.org/10.1016/S1359-6462(00)00669-2.

[35] S. Deng, R. Li, T. Yuan, S. Xie, M. Zhang, K. Zhou, P. Cao, Direct current-enhanced densification kinetics during spark plasma sintering of tungsten powder, Scr. Mater. 143 (2018) 25–29. https://doi.org/10.1016/j.scriptamat.2017.09.009.

[36] J. Kováčik, Correlation between Young’s Modulus and Porosity in Porous Materials, J. Mater. Sci. Lett. 18 (1999) 1007–1010. https://doi.org/10.1023/A:1006669914946.

[37] H. Gietl, J. Riesch, J.W. Coenen, T. Höschen, C. Linsmeier, R. Neu, Tensile deformation behavior of tungsten fibre-reinforced tungsten composite specimens in as-fabricated state,

Fusion Eng. Des. 124 (2017) 396–400. https://doi.org/10.1016/j.fusengdes.2017.02.054.

[38] V. Laws, The efficiency of fibrous reinforcement of brittle matrices, J. Phys. D. Appl. Phys. 4 (1971) 1737–1746. https://doi.org/10.1088/0022-3727/4/11/318.

[39] A. Kelly, G.J. Davies, The principles of the fibre reinforcement of metals, Metall. Rev. 10 (1965) 1–77. https://doi.org/10.1179/mtlr.1965.10.1.1.

[40] Y. Mao, J.W. Coenen, J. Riesch, S. Sistla, J. Almanstötter, B. Jasper, A. Terra, T. Höschen, H. Gietl, C. Linsmeier, C. Broeckmann, Influence of the interface strength on the mechanical properties of discontinuous tungsten fiber-reinforced tungsten composites produced by field assisted sintering technology, Compos. Part A Appl. Sci. Manuf. 107 (2018) 342–353. https://doi.org/10.1016/j.compositesa.2018.01.022.

[41] V. Nikolić, J. Riesch, M.J. Pfeifenberger, R. Pippan, The effect of heat treatments on pure and potassium doped drawn tungsten wires: Part II – Fracture properties, Mater. Sci. Eng. A. 737 (2018) 434–447. https://doi.org/10.1016/j.msea.2018.09.029.

[42] M. Brünig, D. Brenner, S. Gerke, Stress state dependence of ductile damage and fracture behavior: Experiments and numerical simulations, Eng. Fract. Mech. 141 (2015) 152–169. https://doi.org/10.1016/J.ENGFRACMECH.2015.05.022.

[43] H. Gietl, S. Olbrich, J. Riesch, G. Holzner, T. Höschen, J.W. Coenen, R. Neu, Estimation of the fracture toughness of tungsten fibre-reinforced tungsten composites, Eng. Fract. Mech. 232 (2020) 107011. https://doi.org/10.1016/j.engfracmech.2020.107011.